Biophysical Chemistry 146 (2010) 98–107

Contents lists available at ScienceDirect

Biophysical Chemistry

journal homepage: http://www.elsevier.com/locate/biophyschem

Ligand exchange effects in gold nanoparticle assembly induced by oxidative stress biomarkers: Homocysteine and cysteine

Magdalena Stobiecka [a], Jeffrey Deeb [a], Maria Hepel [a,b,*]

[a] Department of Chemistry, State University of New York at Potsdam, Potsdam, NY 13676, USA
[b] Department of Chemistry, State University of New York at Buffalo, Buffalo, NY 14260, USA

ARTICLE INFO

Article history:
Received 25 October 2009
Received in revised form 10 November 2009
Accepted 10 November 2009
Available online 14 November 2009

Keywords:
RELS spectroscopy
Gold nanoparticles
Surface plasmon resonance
Homocysteine-mediated assembly
Oxidative stress biomarkers
Elastic light scattering
Resonance rayleigh scattering

ABSTRACT

The interactions of oxidative stress biomarkers: homocysteine (Hcys) and cysteine (Cys) with the multifunctional gold nanoparticles, important in view of novel biomedical applications in diagnostics and therapy, have been investigated using resonance elastic light scattering (RELS), UV–Vis plasmonic spectroscopy, and high-resolution TEM imaging. The Hcys-induced assembly of gold nanoparticles has been observed for non-ionic surfactant-capped gold nanoparticles as well as for negatively-charged citrate-capped gold nanoparticles. We have observed for the first time the de-aggregation of citrate-capped gold nanoparticle ensembles followed by their conversion to citrate-linked Hcys-capped nanoparticle assemblies. The Cys molecules, which are smaller than Hcys by only one CH_2 group, show much less activity. The mechanisms leading to this intriguing disparity in the abilities of these two thioaminoacids to ligand exchange with surfactant- or citrate-capping molecules of the gold nanoparticle shells are proposed on the basis of the experimental evidence, molecular dynamics simulations, and quantum mechanical calculations. For citrate-capped gold nanoparticles, we postulate the formation of surface complexes facilitated by electrostatic attractions and formation of double hydrogen bonds for both Hcys and Cys. The conformational differences between these two kinds of complexes result in marked differences in the distance between –SH groups of the biomarkers to the gold surface and different abilities to induce nanoparticle assembly. Analytical implications of these mechanistic differences are discussed.

1. Introduction

Biomarkers of oxidative and nitrosative stress have recently been the subject of extensive studies [1,2] as the new evidence demonstrates ever increasing number of related diseases. The oxidative stress has been suggested as the causative factor in aging [3] and many diseases such as cadiovascular, diabetes, cancer, autism spectrum disorders (ASD) [4], and others. Among the biomarkers of oxidative stress are small biomolecules such as: ubiquinol [5] which is very labile in the oxidation of low-density lipoprotein (LDL), glutathione (GSH) which is depleted in the presence of organic radicals and peroxides [6], homocysteine [7,8] which has been found at elevated levels in atherosclerosis [9–14], Alzheimer disease [15,16], dementia [15], and poses an increased risk of birth defects [17]. Some biomarkers of oxidative stress are necessary to maintain healthy homeostasis (e.g. glutathione), while others participate in the development of diseases (e.g. homocysteine). For instance, decreased levels of glutathione and increased levels of oxidized glutathione (GSSG) have been observed in plasma, serum and urine samples from individuals diagnosed with ASD [4,18–20]. Homocysteine (Hcys), which is a sulfur-containing amino acid, is formed during a metabolism of methionine to cysteine but the increased concentration of Hcys in plasma ($C_{Hcys} > 15\ \mu M$) is a risk factor for many disorders, including cardiovascular [9–12], renal [21], Alzheimer's [15,16], and other diseases [22]. Redox-related alterations, measured usually as the change in the concentration ratio of GSH/GSSG which is the main redox level maintaining couple in organisms, may also be heritable. Deviations from healthy biomarker concentration levels may result from deficiency of certain vitamins, e.g. B12 and folic acid (in hyperhomocysteinemia). The investigations of oxidative stress biomarkers are important to understand their behavior and role in organisms and to develop sensors and assays for their rapid detection and diagnosis of stress-related disorders.

The reactivities and interactions of the oxidative stress biomarkers have been investigated in conjunction with the development of molecularly-templated polymer films with biorecognition capabilities designed for biomarkers detection [23], fluorimetric assays based on specific reactions [24–26], electrochemical sensors [27,28], colorimetric assays based on nanoparticle assembly [29–32], and the design of immunosensors [33] and other sensors for the analysis of biomarkers or utilizing biomarkers in the sensory film design [34–36]. In particular, in studies of biomolecule-induced gold nanoparticle assembly, the kind of interparticle interactions is the key element of the functionalized nanoparticle self-affinity [37–39]. The interparticle forces include electrostatic [40], zwitterionic [29,40], van der Waals

* Corresponding author. Department of Chemistry, State University of New York at Potsdam, Potsdam, NY 13676, USA. Tel.: +1 315 267 2264; fax: +1 315 267 3170.
E-mail address: hepelmr@potsdam.edu (M. Hepel).

0301-4622/$ – see front matter © 2009 Elsevier B.V. All rights reserved.
doi:10.1016/j.bpc.2009.11.001

forces [41], as well as hydrogen bonding forces [41–43]. The investigations of functionalized spherical gold nanoparticles and gold nanorods for application in novel assays for GSH [43], cysteine [32,44–48] and homocysteine [29,30,45,49] have been reported. The gold nanoparticle cores with protective shells of self-assembled monolayers (SAM) of thiolates [50,51], surfactants [47,52,53], citrate ions [48], and others can be utilized in the analysis. A difference in the sensitivity of the gold nanoparticle assembly process to structurally similar cysteine and homocysteine molecules, which differ only by one CH_2 group, has been found [32,46,47]. Probing the interactions of biomolecules with gold nanoparticles and their influence on surface plasmon resonance and the elastic light scattering cross-section has potential applications in the development of novel assays for these molecules.

The gold nanoparticle assembly process observed upon the addition of biomolecules is believed to be due to the ligand exchange [54] followed by the attractive interparticle interactions [29,48]. According to the thermodynamic stability, the citrate shell is less strongly bound than cysteine shell and the latter is less strongly bound than homocysteine shell. In practice, the kinetic hindrance may slow down considerably the ligand exchange processes. Also, the interparticle molecular-linking may induce an assembly before the completion of a ligand exchange process, as we have recently observed in the case of GSH-induced assembly.

The biomolecule-induced gold nanoparticle assembly process can be monitored using surface plasmon absorbance band shifts. The oscillation frequency of the local surface plasmon (SP) is very sensitive to the changes in dielectric environment of nanoparticles and distance between nanoparticles within 5*r* range (where *r* is the nanoparticle radius). Theoretical studies of plasmonic oscillations [55–65] and SP absorbance spectra [66–74] have enabled the understanding of mechanisms leading to the absorbance maximum shifts associated with the assembly processes. The hydrodynamic radius of nanoparticle aggregates can be measured using dynamic light scattering although the complex dielectric medium and formation of aggregates of small particles may complicate the analysis. The use of transmission electron microscopy (HR-TEM) has been so far the best in determining the nanoparticle diameters and presenting images of aggregated nanoparticles. In this work, we have applied UV–Vis plasmonic absorbance measurements, HR-TEM, and the resonance elastic light scattering (RELS) spectroscopy [75–87]. The latter provides very sensitive measure of the degree of gold nanoparticle assembly. The gold nanoparticles show enhanced scattering during the assembly process due to the collective oscillation of local surface plasmons in nanoparticles bound in an ensemble.

In this work, the assembly of gold nanoparticles induced by oxidative stress biomarkers, homocysteine and cysteine, has been investigated using non-ionic fluorosurfactant-capped gold nanoparticles and negatively-charged citrate-capped gold nanoparticles. The remarkable differences in ligand exchange abilities of the homocysteine and cysteine, have been observed for both the charged and uncharged nanoparticle shells. Different mechanisms leading to these effects for uncharged and charged nanoparticle shells are proposed. The elucidation of these mechanisms is crucial for analytical determination of structurally similar cysteine and homocysteine using rapid and inexpensive measurement techniques important for oxidative stress screening and prevention of environmental pollution effects on human health.

2. Experimental

2.1. Chemicals

All chemicals used for investigations were of analytical grade purity. DL-Homocysteine ($HS(CH_2)_3NH_2COOH$), L-Cysteine ($HS(CH_2)_2NH_2COOH$), tetrachloroauric(III) acid trihydrate ($HAuCl_4 \cdot 3H_2O$) with 99.9+% metals basis, D-Methionine,and L-glutathione (GSH) reduced (minimum 99%), were purchased from Sigma Aldrich Chemical Company (Atlanta, GA, U.S.A.) and used as received. ZONYL FSN-100, a fluorocarbon-ether surfactant (FES), with nominal composition $CF_3(CF_2)_m(C_2H_4O)_nCH_2OH$ and average molecular mass M = ~950 g/mol was obtained from Sigma Aldrich. Sodium citrate dihydrate ($HOC(COONa)(CH_2COONa)_2 \cdot 2H_2O$) was received from J.T. Baker Chemical Co. (Phillipsburg, NJ, U.S.A.). Sodium borohydride ($NaBH_4$) was obtained from Fisher Scientific Company. L(+) Histidine was purchased from Eastman Organic Chemicals (Rochester, NY, U.S.A.). Solutions were prepared using Millipore (Billerica, MA, U.S.A.) Milli-Q deionized water (conductivity $\sigma = 55$ nS/cm). They were deoxygenated by bubbling with purified argon.

2.2. Apparatus

The imaging analyses of Au nanoparticles were performed using high-resolution transmission electron microscopy (HR-TEM) with Model JEM-2010 (Jeol, West Chester, PA, U.S.A.) HR-TEM instrument (200 kV) and imaging with a Jeol Model JSM-7400F field-emission scanning electron microscope (FE-SEM). The elastic light scattering spectra were recorded using LS55 Spectrometer (Perkin Elmer, Waltham, MA, U.S.A.) equipped with 20 kW Xenon light source operating in 8 μs pulsing mode. Pulse width at half height was less than 10 μs. Separate monochromators for the incident beam and the detector beam enabled to use monochromatic radiation with wavelengths from 200 nm to 800 nm with 1 nm resolution. Additionally, the system was equipped with sharp cut-off filters: 290, 350, 390, 430, 515 nm. The dual detector system consisted of a photomultiplier tube (PMT) and an avalanche photodiode. The RELS spectra were obtained at 90° angle from the incident (excitation) light beam. The excitation beam monochromator was either scanned simultaneously with the detector beam monochromator ($\Delta\lambda = 0$) or set at a constant excitation wavelength. The UV–Vis spectra were recorded using Perkin Elmer Lambda 50 Spectrophotometer in the range 400 to 900 nm or Ocean Optics (Dunedin, FL, U.S.A.) Model R4000 Precision Spectrometer in the range from 340 nm to 900 nm.

2.3. Procedures

The Au nanoparticles were synthesized according to the published procedure [88]. Briefly, to obtain 5 nm AuNP, 10 mM $HAuCl_4$ was mixed with 10 mM trisodium citrate solution (ratio 1: 3.75) and poured to distilled water (109 mL). The obtained solution was vigorously stirred and fresh cold $NaBH_4$ solution (5 mM, 8.9 mL) was added dropwise. The solution slowly turned light grey and then ruby red. Stirring was maintained for 30 min. The obtained citrate-capped core-shell Au nanoparticles (AuNP) were stored at 4 °C. Their size, determined by HR-TEM imaging and UV–Vis surface plasmon absorption was 5.0 nm. The concentrations of AuNP's are given in moles of particles per 1 L of solution (usually, in the nM range). The RELS and UV–Vis spectra for samples were obtained with 1 min of mixing of AuNP with biomolecule solutions, unless otherwise stated.

Quantum mechanical calculations of electronic structures for a model fluorocarbon-ether surfactant, citric acid, cysteine and homocysteine were performed using modified Hartree–Fock methods [89,90] with 6–31G* basis set and pseudopotentials, semi-empirical PM3 method, and density functional theory (DFT) with B3LYP functional. The molecular dynamics simulations and quantum mechanical calculations were carried out using procedures embedded in Wavefunction (Irvine, CA, U.S.A.) Spartan 6. The electron density and local density of states (LDOS) are expressed in atomic units, au^{-3}, where 1 au = 0.529157 Å and 1 au^{-3} = 6.749108 $Å^{-3}$.

3. Results and discussion

3.1. Plasmonic spectroscopy of thioaminoacid-induced assembly of gold nanoparticles protected by ZONYL

Fluorosurfactants provide similar advantages to other surfactants but, in addition, show high degree of chemical inertness. For these reasons they have recently been applied in chemical analysis [52]. The ZONYL fluorosurfactant is known to form self-assembled monolayers on gold surfaces rendering the surface more hydrophobic and significantly retarding the gold oxide formation processes [91]. In the case of AuNP, it stabilizes gold colloids by forming tight shells around nanoparticle cores with hydrophilic heads oriented toward Au surface and fluorocarbon tails forming hydrophobic non-interacting external surface. Although this surfactant forms water-tight shells, its bonding to a gold surface is not as strong as that of thiolates. Therefore, in their presence, ZONYL is replaced in a ligand exchange process by thiols, including thioaminoacids, homocysteine and cysteine, investigated in this work, provided that sufficiently high concentration of these agents is used and long enough time is allowed. The HR-TEM images of fluorosurfactant-capped AuNP's are presented in Fig. 1 before (a) and after (b–d) homocysteine-induced nanoparticle framework assembly.

The ligand exchange process taking place upon addition of homocysteine to ZONYL-capped AuNP can be monitored using SP-band absorbance of AuNP, as illustrated in Fig. 2. The UV–Vis spectra 1–9 were recorded for increasing concentrations of Hcys, from 0 to 22.2 μM and constant concentration of $AuNP_{5\ nm}$ (6 nM). It is seen that the SP band shifts toward longer wavelengths and the maximum absorbance increases with increasing C_{Hcys}. These observations are consistent with ligand exchange process:

$$AuNP/FES_x + yHcys = AuNP/Hcys_y + xFES$$

where $x \approx y$, followed by interparticle molecular linking of AuNP/Hcys through direct Hcys-Hcys interactions. At the pH of these experiments (pH = 6.0), homocysteine exists as a zwitterion with α-amino group protonated ($-NH_3^+$) and carboxylic group dissociated (COO^-). Therefore, the zwitterionic interparticle binding between Hcys-capped AuNP is playing a predominant role as recently discussed by Zhong et al. [29].

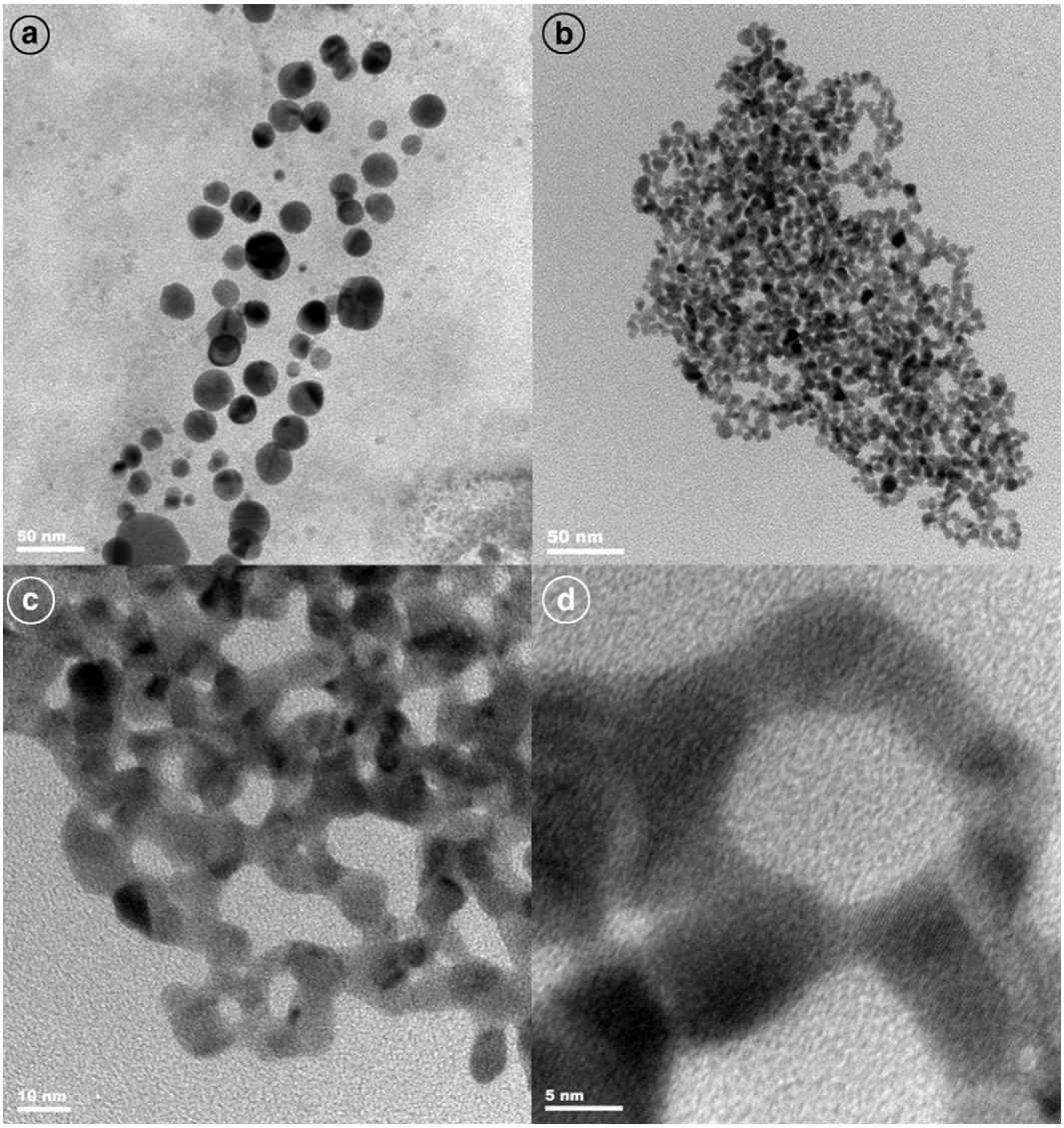

Fig. 1. HR-TEM images of ZONYL-capped gold nsanoparticles before (a) and after assembly with 15 μM homocysteine (b–d); $C_{AuNP} = 6$ nM, $C_{ZONYL} = 0.22$ %, pH = 6; bar size: (a) 50 nm, (b) 50 nm, (c) 10 nm, (d) 5 nm.

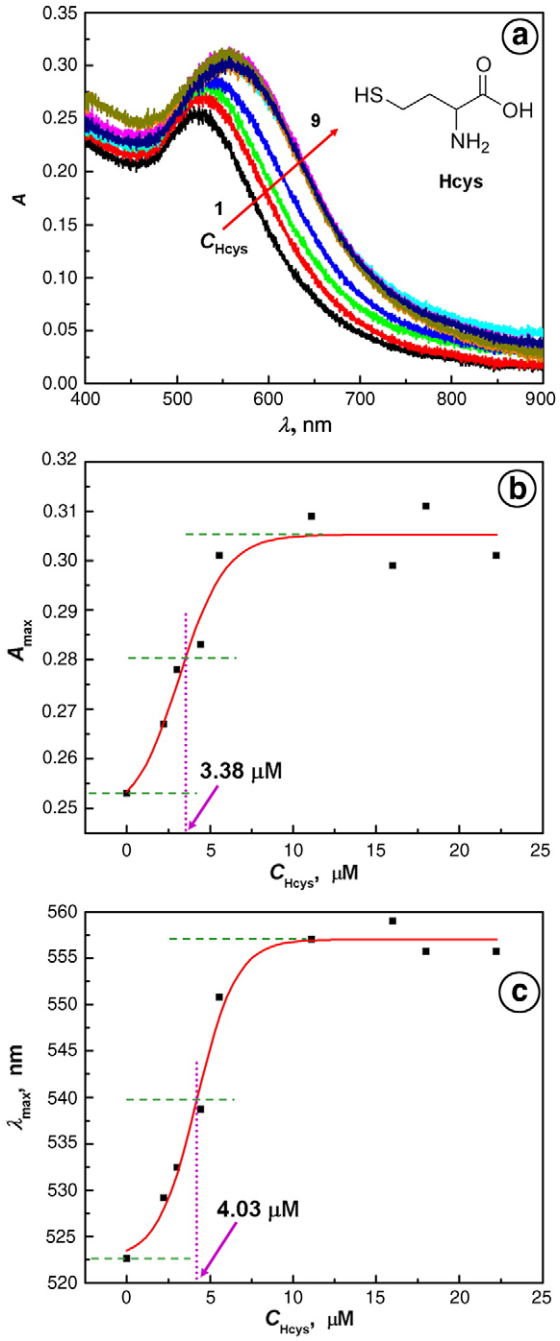

Fig. 2. (a) Absorbance spectra for ZONYL-capped AuNP for different concentrations of homocysteine, C_{Hcys} [μM]: (1) 0, (2) 2.22, (3) 3, (4) 4.44, (5) 5.56, (6) 11.11, (7) 16, (8) 18, (9) 22.22. C_{AuNP} = 6 nM, C_{ZONYL} = 0.22 %, pH = 6; (b–c) dependence of (b) λ_{max} and (c) A_{max} vs. C_{Hcys}.

The bathochromic shift of the surface plasmon peak ($\Delta\lambda_{max}$ = 36 nm, for 16 μM Hcys) corresponds to the formation of small Hcys-linked AuNP ensembles. The increase of SP absorbance by 21% (from 0.253 to 0.305, Fig. 1b) indicates on the collective oscillations of local surface plasmons in AuNP that form these ensembles. The collective oscillation of local surface plasmons is excited when the distance d between AuNP is: $d<5r$, where r is the AuNP radius. The absorbance maximum increases with C_{Hcys} and reaches the saturation value at $C_{Hcys}>7$ μM, with the half-absorbance change appearing at C_{Hcys} = 3.38 μM. The value of λ_{max} also reaches saturation at $C_{Hcys}>7$ μM (Fig. 1c). Therefore, we can assume that above 7 μM Hcys concentration the ligand exchange process has completed and nanoparticle shells are saturated with Hcys.

Extensive studies of the surface plasmon absorbance for various AuNP systems have been carried out by several groups [37,38,42,50,51,70,86,92–99]. In particular, it follows from studies of the homocysteine-mediated assembly of AuNP that the interparticle zwitterion interaction of the Hcys-Au system is particularly strong [29] and that the Hcys-mediated assembly of AuNP can be accelerated by an increased temperature and ionic strength of the solution thus reducing the barrier for Hcys attachment to gold nanoparticle surface [29]. Also, the assembly can be reversed by the pH change [29,30].

Similar experiments performed with cysteine indicate that at higher concentrations ($C>15$ μM) the kinetics of ligand exchange for both Hcys and Cys is very fast and the exchange is completed within 1 min of mixing AuNP solution with the thioaminoacids. However, at lower concentrations, the ligand exchange is considerably faster for Hcys than for Cys.

3.2. Resonance scattering of the thioaminoacid-mediated ZONYL-capped gold nanoparticle assembly process

Typical light scattering spectrum for a ZONYL FSN surfactant-capped 5 nm diameter Au nanoparticles ($AuNP_{5\ nm}$) in solution is presented in Fig. 3, curve 1, for $AuNP_{5\ nm}$ concentration of 6 nM and a constant excitation wavelength λ_{ex} = 550 nm (1.94 eV). The strong resonant Rayleigh scattering from $AuNP_{5\ nm}$ nanoparticles in solution results from the absorption of photons at 550 nm followed by secondary emission without any energy loss. Thus, the coherent elastic Rayleigh scattering with Gaussian peak shape centered at $\lambda_{em} = \lambda_{ex}$ = 550 nm is observed. The narrow linewidth of $\Delta\lambda$ = 15 nm confirms that the effects due to radiation broadening, density fluctuation, fluorescence, and inelastic Raman scattering are negligible. Note that the background intensity is very low (virtually zero), which is leading to the well defined RELS peaks.

The addition of homocysteine to the ZONYL-capped $AuNP_{5\ nm}$ nanoparticles results in strong enhancement of Rayleigh scattering, as indicated in Fig. 3, curves 2–9, obtained for 6 nM $AuNP_{5\ nm}$ + x μM Hcys, where x = 0 ... 22.2 μM. Upon addition of Hcys, the solution pH was maintained at pH = 6.0. This pH value is within the range of predominantly neutral (zwitterionic) form of homocysteine (pH = 2.22 to 8.87; $pK_{a,1}$ = 2.22 (COOH), $pK_{a,2}$ = 8.87 (NH_2), $pK_{a,3}$ = 10.86 (SH)). The strong enhancement of RELS from $AuNP_{5\ nm}$ by Hcys molecules is expected since any size increase of AuNP due to the aggregate formation associated with interparticle interactions with zwitterionic Hcy-Hcys cross-linking should result in stronger scattering. The strong sixth-power dependence of elastic scattering intensity I_{sc} on the

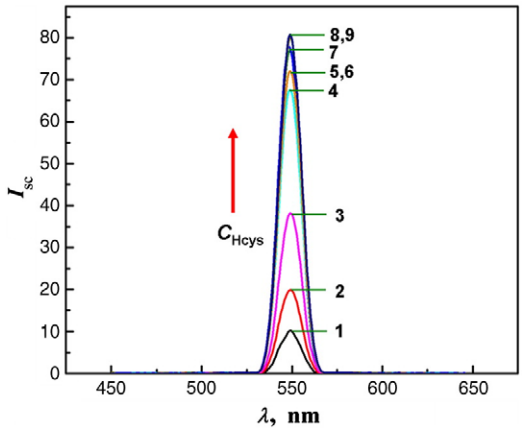

Fig. 3. Resonance elastic light scattering spectra for ZONYL-capped $AuNP_{5\ nm}$ for different concentrations of homocysteine, C_{Hcys} [μM]: (1) 0, (2) 2.22, (3) 3, (4) 4.44, (5) 5.56, (6) 14, (7) 16, (8) 18, (9) 22.22. C_{AuNP} = 6 nM, C_{ZONYL} = 0.22 %, pH = 6, λ_{ex} = 550 nm.

nanoparticle diameter a follows from the Rayleigh equation for light scattering from small particles:

$$I_{sc} = I_0 N \frac{\left(1 + \cos^2\theta\right)}{2R^2}\left(\frac{2\pi}{\lambda}\right)^4 \frac{\left([n_2-n_1]^2-1\right)}{\left([n_2-n_1]^2+2\right)}\left(\frac{a}{2}\right)^6 \quad (1)$$

where n_1 and n_2 are the refractive indices for the solution and particles, respectively, λ is the wavelength of incident light beam, θ is the scattering angle, N is the number of particles, and I_0 is the constant. For λ = const and other experimental conditions (θ, R, I_0) unchanged, one obtains:

$$\frac{I_{sc,2}}{I_{sc,1}} = \frac{N_2 a_2^6}{N_1 a_1^6} = c_{rel} a_{rel}^6 \quad (2)$$

where indices 1,2 stand for the particles before and after Hcys addition, respectively, $c_{rel} = N_2/N_1$ is the relative concentration of particles after addition of Hcys, and $a_{rel} = a_2/a_1$ is the relative diameter of particles after addition of Hcys. Therefore, the increase in the particle diameter can be estimated as follows:

$$a_{rel} = \left[\frac{I_{sc,2}}{c_{rel} I_{sc,1}}\right]^{1/6} \quad (3)$$

Furthermore, the relative concentration c_{rel}, which is equal to 1 for a no-aggregation condition and less than 1 for aggregation, can be expressed by:

$$c_{rel} = \frac{N_2}{N_1} = \frac{V_1}{V_2} \quad (4)$$

where V_i is the effective volume of a single aggregate i. Substituting $V_i = (4/3)\pi(a_i/2)^3$, one obtains:

$$c_{rel} = a_{rel}^{-3} \quad (5)$$

and:

$$\frac{I_{sc,2}}{I_{sc,1}} = a_{rel}^3 \quad (6)$$

Therefore, the increase of the particle diameter can be estimated as follows:

$$a_{rel} = \sqrt[3]{\frac{I_{sc,2}}{I_{sc,1}}} \quad (7)$$

From the data of Fig. 3, the scattering intensity increase is: $I_{sc,2}/I_{sc,1} = 80.44/10.26 = 7.84$ and, hence,

$$a_{rel} = 1.99 \quad (8)$$

This means that most likely small aggregates composed of only few nanoparticles (e.g. 2–6) are formed. Since a small contribution to the change in particle diameter is also due to the ligand exchange, we have to estimate this contribution. The thickness of the ZONYL shell around AuNP is 1.1 nm (vertical, fully extended orientation, ZONYL FSN-100, with formula $CF_3(CF_2)_m(C_2H_4O)_nCH_2OH$ and average $m = 12$, $n = 6$ assumed on the basis of molmass $M = 950$ g/mol) and the height of Hcys molecule adsorbed on Au is on the order of 0.5 nm based on quantum mechanical evaluation for Hcys adsorbed on a solid Au surface. The structure and dimensions of ZONYL and Hcys molecules are shown later on (Figs. 8–11). Hence, the diameter of a single AuNP, with core of 5 nm diameter would decrease from ca. 7.2 nm to 6.0 nm. Obviously, the diameter decrease cannot explain the observed ~8-fold scattering intensity increase. Therefore, we can conclude that Hcys-mediated assembly of AuNP's occurs upon addition of Hcys to the ZONYL-capped AuNP solution and the effective diameter of assemblies is: $a = 1.99\, a_0$ (where a_0 is the diameter of Hcys-capped AuNP). This assembly results in a large increase in I_{sc} in accord with the data of Fig. 3. Because there are only very weak interactions between the Hcys molecules and hydrophobic tail of ZONYL, any Hcys-mediated bridging of ZONYL-capped AuNP's, such as that observed upon addition of GSH to citrate-capped AuNP's, cannot take place. Hence, the ligand exchange is the first stage of the interactions between Hcys and ZONYL-capped AuNP and it is followed by Hcys-Hcys interparticle interactions leading to AuNP assembly.

3.3. Ligand exchange processes for ZONYL-capped gold nanoparticles

It is interesting to compare the ligand exchange processes for different aminoacid ligands and ZONYL-capped AuNP. As reported earlier [24,52], these processes differ considerably between aminoacids and these differences are due to highly selective ZONYL-replacement abilities of the particular aminoacids. The plots of RELS intensity vs. aminoacid concentration measured at $\lambda_{ex} = 550$ nm for Hcys, methionine, alanine, histidine, and glutathione, are presented in Fig. 4. They show a strong increase of I_{sc} with C for homocysteine and apparent no response for other aminoacids and glutathione. The I_{sc} vs. C_{Hcys} dependence is sigmoidal with an inflection point at low Hcys concentration indicating a high affinity of Hcys for Au surface, higher than that of ZONYL. From a Boltzmann function fitted to the experimental data for Hcys and ZONYL, we obtain:

$$I_{sc} = A_2 + (A_1 - A_2)/(1 + \exp[(C - C_{1/2})/s]) \quad (9)$$

where A_1, A_2 — are the lower and higher I_{sc} plateaus, $C_{1/2}$ is the concentration at the inflection point, and s is the slope parameter. The value of $C_{1/2} = 3$ μM and the characteristic constant $K^*_{1/2}$ describing the "half-reaction" state of the ligand exchange in the ZONYL replacement by Hcys is: $K^*_{1/2} = 3.3 \times 10^5\ M^{-1}$ (note that the value and units of this phenomenological half-reaction-state equilibrium constant are typically different than those for a thermodynamic equilibrium constant for higher order reactions involving more than single molecules). The high value of $K^*_{1/2}$ confirms a high affinity of Hcys to the gold surface in comparison to that of the ZONYL surfactant.

The longer elution time for Hcys than for Cys observed in C18 column chromatography experiments [24,52] is consistent with higher affinity of Hcys than Cys to hydrophobic chains. In the setting of a ZONYL-capped AuNP, this would translate to a slower transfer of Hcys through a ZONYL shell and a slower kinetics of the ligand

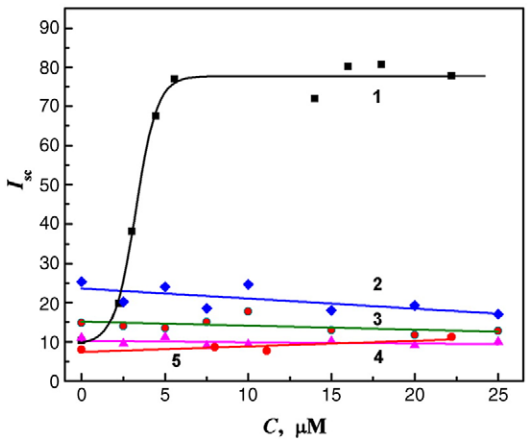

Fig. 4. Dependence of elastic light scattering intensity maximum $I_{sc,max}$ for ZONYL-capped AuNP on concentration of analytes: (1) homocysteine, (2) methionine, (3) alanine, (4) histidine, (5) glutathione, $C_{AuNP} = 6$ nM, $C_{ZONYL} = 0.22\%$, pH = 6, $\lambda_{ex} = 550$ nm.

exchange process. Since the opposite is observed, this means that other factors play a role in the ligand exchange mechanism. The interactions of Hcys and Cys with ZONYL molecules are further discussed later on by employing molecular dynamic simulations of a model ZONYL and biomarker molecules.

3.4. Interactions of thioaminoacids with citrate ligands of core-shell gold nanoparticles

Upon addition of homocysteine to citrate-capped AuNP, an increase in resonance elastic light scattering, similar to the one described for ZONYL-capped AuNP, is also observed (Fig. 5), provided that the solution pH is carefully controlled. The RELS spectra in Fig. 5 were obtained at pH = 5.0 for $\lambda_{ex} = 560$ nm, for increasing concentrations of Hcys from $C_{Hcys} = 0$ to 15 μM. The increase in scattering intensity upon addition of 15 μM Hcys is $I_{sc,2}/I_{sc,1} = 36.2/1.91 = 19.0$ (mean of 5 measurements). The 19-fold increase in scattering intensity clearly indicates on the homocysteine-induced assembly of AuNP. Utilizing again Eq. (7), we obtain for the increase of particle diameter: $a_{rel} = 2.7$.

Similar RELS experiments carried out for other aminoacid ligands and glutathione, presented in Fig. 6, show that the RELS response is highly selective to Hcys, consistent with recent findings [29,43,46] showing that thiol-containing aminoacids adsorb preferentially on a gold surface while glutathione (at neutral pH) is repelled from the citrate shell of nanoparticles. The mechanisms leading to this high selectivity are not well understood, though the importance of this selectivity for analytical determinations of homocysteine in a matrix of aminoacids and glutathione is high.

In order to explore the effects of protonation equilibria for species in solution and in the protective SAM environment of gold nanoparticle shells, we have performed RELS measurements for Hcys and citrate-capped AuNP at three different solution pH: 2.0, 5.0, and 9.0. The plot of scattering intensity I_{sc} vs. C_{Hcys} for these three media is presented in Fig. 7. The three dependencies of I_{sc} vs. C_{Hcys} for different pH values show completely different behaviors. The curve 1 for pH = 2.0 shows a scattering intensity decrease with increasing C_{Hcys} and establishment of a plateau for $C_{Hcys} > 4$ μM. Curve 2 shows a sigmoidal shape with the onset of scattering at $C_{Hcys} = 5$ μM and establishment of a new level of scattering intensity plateau for $C_{Hcys} > 7$ μM. In the case of the third curve, for pH = 9.0, there is virtually no scattering change seen for the entire concentration range of Hcys examined and the level of scattering is very low ($I_{sc} \approx 8$, for 20 μM Hcys). Note that the scattering intensity levels established for pH = 2.0 and pH = 5.0 at higher concentrations of Hcys, are different.

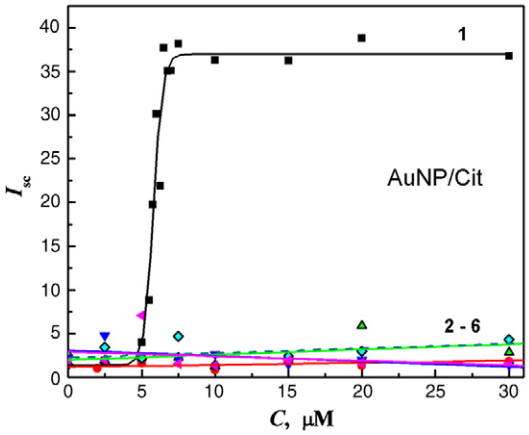

Fig. 6. Dependence of elastic light scattering intensity maximum $I_{sc,max}$ for citrate-capped $AuNP_{5\ nm}$ on concentration of analytes: (1) homocysteine, (2) methionine, (3) alanine, (4) histidine, (5) glutathione, (6) cysteine, $C_{AuNP} = 3.8$ nM, pH = 5, $\lambda_{ex} = 560$ nm.

The elucidation of the mechanism of processes leading to the complex behavior of the citrate-capped AuNP – homocysteine system is a key element to understanding the reactivity and assembling properties of functionalized AuNP and their interactions with small biomolecules. The three situations represented by the data of Fig. 7 can be analyzed as follows:

(i) The low elastic scattering intensity observed at pH = 9 (curve 3) for all Hcys concentrations examined is certainly due to the high gold colloid stability which is associated with strong electrostatic interparticle repulsions between deprotonated carboxyl groups that exist in the citrate shell before and in the Hcys-shell after the ligand exchange has taken place.

(ii) The situation changes at pH = 5 (curve 2) where citrates are still predominantly deprotonated ($pK_{a,1} = 3.09$, $pK_{a,2} = 4.75$, $pK_{a,3} = 5.41$) but homocysteine exists as a zwitterion with protonated $-NH_3^+$ group and dissociated COO^- group ($pK_{a,1} = 2.22$ (COOH), $pK_{a,2} = 8.87$ (NH_2)). Thus, at low Hcys concentrations ($C_{Hcys} < 5$ μM), scattering is low since it is dominated by interparticle repulsions of negatively-charged citrate shells. As the ligand exchange process progresses, the citrate ions are being replaced by the neutral Hcys molecules. The progression is accelerated at higher Hcys concentrations. The switch from low elastic light scattering intensity to high intensity is observed in the concentration range: 5 μM < C_{Hcys} < 7 μM. At $C_{Hcys} = 7$ μM, the

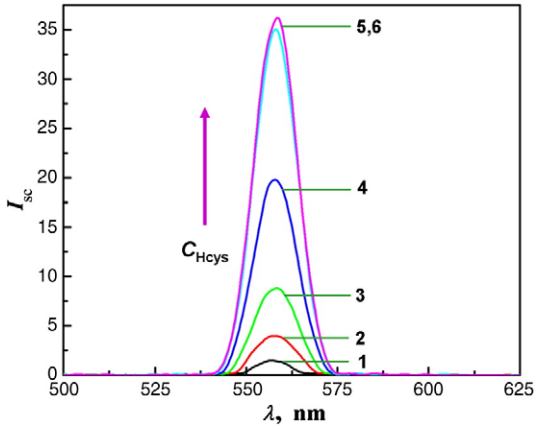

Fig. 5. Resonance elastic light scattering spectra for citrate-capped $AuNP_{5\ nm}$ for different concentrations of homocysteine, C_{Hcys} [μM]: (1) 0, (2) 5, (3) 5.5, (4) 5.75, (5) 6.75, (6) 15, $C_{AuNP} = 3.8$ nM, pH = 5, $\lambda_{ex} = 560$ nm.

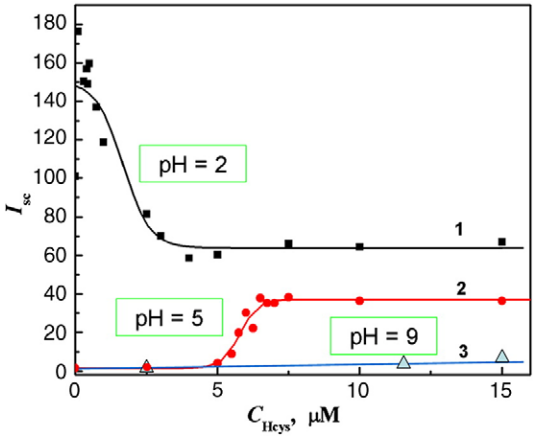

Fig. 7. Dependence of elastic light scattering intensity maximum $I_{sc,max}$ on concentration of homocysteine C_{Hcys} for citrate-capped $AuNP_{5\ nm}$ for different solution pH: (1) pH = 5 and (2) pH = 2.

saturation level is attained. This level can be ascribed to small ensembles of Hcys-linked AuNP where the interparticle attractions are attributed to strong Hcys-Hcys zwitterionic interactions.

(iii) In an acidic solution at low pH (curve 1, pH = 2) and in the absence of homocysteine, a strong scattering intensity is observed which is due to the extensive interparticle hydrogen bonding. This occurs because at this pH citrates are predominantly undissociated ($pK_{a,1} = 3.09$, $pK_{a,2} = 4.75$, $pK_{a,3} = 5.41$, for citric acid) rendering the gold colloid unstable. The hydrogen bonding is responsible for the formation of gold nanoparticle networks and since the scattering intensity strongly increases with the aggregate size, a high scattering intensity is observed. Upon the addition of homocysteine, the light scattering intensity unexpectedly decreases to a new level, approximately at 50% of the initial scattering intensity value. This can be rationalized by assuming the dismantling of the initial citrate-linked gold nanoparticle ensembles and replenishing the nanoparticle shells with homocysteine in a ligand exchange process. While the newly formed shells are more strongly bound to the gold cores than citric acid based shells do, the Hcys molecules at pH = 2 are partially positively charged and cannot form as large the nanoparticle aggregates as citrate-capped AuNP do. In fact, one should expect interparticle repulsions of Hcys-capped AuNP at pH = 2 since $pK_{a,1} = 2.22$ (COOH), $pK_{a,2} = 8.87$ (NH_2) for homocysteine. There are two plausible explanations of this behavior. On one hand, the reported value of $pK_{a,1}$ for Hcys, which has been determined for the solution phase, is not relevant to Hcys molecules adsorbed on gold. A shift of the value of $pK_{a,1}$ to somewhat lower values, would make the Hcys molecules still zwitterionic at pH = 2. However, to evaluate this possibility, the pK_a values for surface bound homocysteine should be determined. On the other hand, some of the partially dissociated citrate molecules may participate in the neutralization and cross-linking of Hcys-capped AuNP. The level of light scattering intensity indicates that the nanoparticle ensembles formed are larger than those formed at pH = 5 where pure zwitterionic interactions have been found. Therefore, participation of citrate ligands in the gold nanoparticle cross-linking is likely to occur.

In summary, we have observed for the first time the scattering spectra for the de-aggregation of citrate-capped gold nanoparticle ensembles followed by their conversion to citrate-linked Hcys-capped nanoparticle assemblies.

3.5. Molecular dynamics and quantum mechanical analysis of ligand exchange processes for core-shell gold nanoparticles

The two main monolayer-protective types of shells for AuNP examined in this work differ considerably in their composition and properties, yet they both provide selectivity toward homocysteine versus cysteine in the nanoparticle assembly process. In order to elucidate the intriguing difference one methylene group makes in the behavior of cysteine (HS–$(CH_2)_2$–NH_2–COOH) and homocysteine (HS–$(CH_2)_3$–NH_2–COOH), we have performed molecular dynamics and quantum mechanical calculations to characterize the kind of intermediate structures that form on approach of Cys and Hcys molecules to a charged citrate-capped gold nanoparticle. Molecular dynamics simulations have also been carried out to evaluate the interactions of Hcys and Cys with a non-ionic fluorosurfactant-capped gold nanoparticle.

A model gold nanoparticle coated with a monolayer of a fluorocarbon-ether surfactant is presented in Fig. 8. The fluorosurfactant used for model calculations has a composition $CF_3(CF_2)_m(C_2H_4O)_nH$ and consists of a hydrophobic fluorocarbon tail and an ethoxylated chain $–(C_2H_4O)_n–$, with assumed chain lengths: $m = 6$ and $n = 4$. The formation of a tight hydrophobic shell is consistent with the ZONYL-AuNP core-shell structure following studies on Au solid

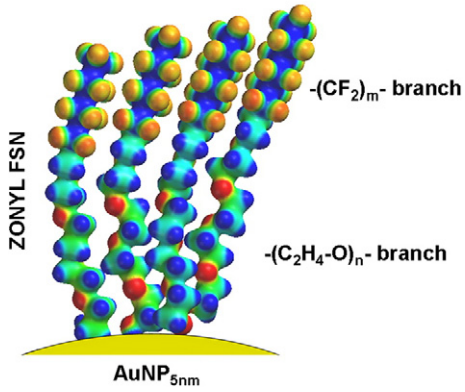

Fig. 8. Model ZONYL-capped gold nanoparticle; electron density surfaces for $d = 0.08$ au^{-3}, calculated for a fluorosurfactant molecule with formula $CF_3(CF_2)_m(C_2H_4O)_nH$ with $m = 6$, $n = 4$, with electrostatic potential map (color coded from negative — red, to positive — blue).

electrode surfaces [91]. In order to understand the behavior of cysteine and homocysteine in the surroundings of a fluorosurfactant shell, we have performed molecular dynamics simulations of the interactions of a biomarker with different parts of the fluorosurfactant molecule: (a) the top $–CF_3$ group of the molecule, (b) the side of the $–(CF_2)_m–$ tail, and (c) the side of the ethoxy chain. In Fig. 9, shown are cysteine molecules interacting with a fluorosurfactant molecule at these three positions. While there is virtually no effect of cysteine on the conformation of the fluorosurfactant molecule when cysteine interacts at the top or at the side of the hydrophobic tail, there is a change of the conformation observed when cysteine interacts with the ethoxylated part of the fluorosurfactant. A tendency of the ethoxy chain toward surrounding the cysteine molecule is observed in later stages of the simulation. Similar molecular dynamics simulations were performed for homocysteine. Fig. 10 illustrates the interactions of homocysteine with the top of the surfactant molecule, the side of the hydrophobic tail and the side of the ethoxylated chain. Again, there are no conformational changes in the surfactant molecule when homocysteine interacts with the hydrophobic tail. There are some

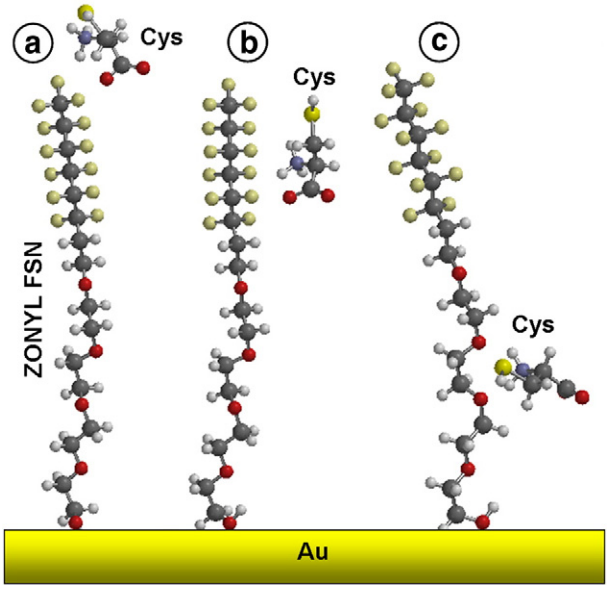

Fig. 9. Molecular dynamics simulations of interactions of cysteine with a model fluorosurfactant molecule with formula CF3(CF2)m(C2H4O)nH with $m = 6$, $n = 4$; positions of cysteine: (a) at the top of the surfactant molecule, (b) at the side of the hydrophobic –(CF2)m– chain, and (c) at the side of ethoxy chain.

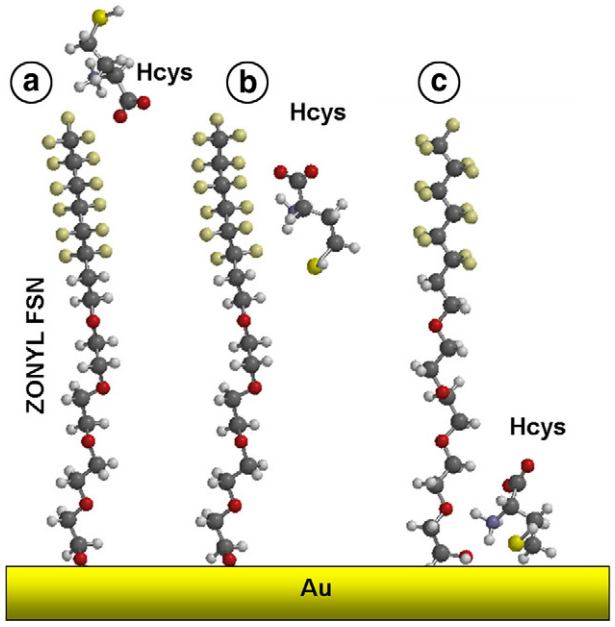

Fig. 10. Molecular dynamics simulations of interactions of homocysteine with a model fluorosurfactant molecule with formula CF3(CF2)m(C2H4O)nH with $m=6$, $n=4$; positions of homocysteine: (a) at the top of the surfactant molecule, (b) at the side of the hydrophobic –(CF2)m– chain, and (c) at the side of ethoxy chain.

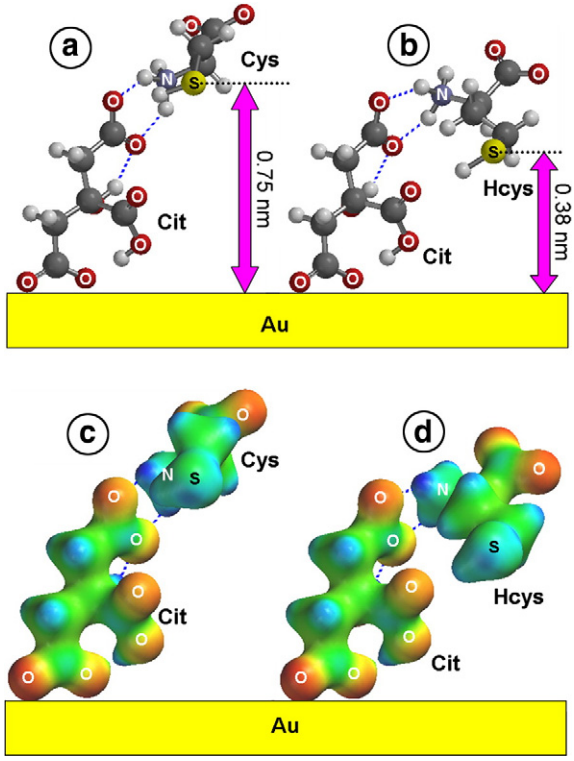

Fig. 11. Interactions of cysteine and homocysteine with citrate ions in a ligand exchange process: (a, b) surface complex formation through hydrogen bonding calculated for (a) Cit-Cys and (b) Cit-Hcys using molecular dynamics, and (c, d) electron density surfaces for $d=0.08$ au^{-3}, with electrostatic potential map for (c) Cit-Cys and (d) Cit-Hcys; electrostatic potential: color coded from negative – red to positive – blue.

conformational changes in the surfactant molecule when homocysteine interacts with ethoxyleted chain, but these changes are much smaller than in the case of cysteine. This may be due to higher polarization of cysteine than homocysteine. The ethoxylated chain attempts to surround the smaller cysteine molecule while lowering the system energy. Therefore, it seems that the stronger interaction of cysteine with the fluorosurfactant may slow down considerably the adsorption competition between cysteine and fluorosurfactant at the surface of an Au substrate and hinder the ligand exchange process. It has been suggested earlier that the stronger affinity of homocysteine to fluorocarbon tail facilitates faster transport of homocysteine than cysteine, which is however, contradicted by the results of C18 column chromatography experiments [52] showing clearly faster elution of Cys than Hcys, consistent with stronger interactions of Hcys with a hydrophobic chain [24]. In addition to that, the shorter cysteine forms less strongly bound film of SAM on gold than longer homocysteine so in the adsorption competition, cysteine is a weaker competitor to the fluorosurfactant than homocysteine. In summary, there seem to be both thermodynamic as well as kinetic aspects of the ligand exchange between the thioaminoacids and the fluorosurfactant that lead under carefully selected conditions to a much higher effectiveness of homocysteine, in relation to that of cysteine, in replacing ZONYL from the gold nanoparticle protective shell.

The interactions of cysteine and homocysteine with citrate-capping film have also been considered. At the pH of measurements (pH 5–6), the citrate shell is charged negatively providing a long-term stability for the gold colloid, whereas both cysteine and homocysteine are in the form of zwitterions with protonated $-NH_3^+$ group and dissociated $-COO^-$ group. The main interaction of the electrostatic nature between $-COO^-$ group of the nanoparticle shell and $-NH_3^+$ group of the approaching thioaminoacid is expected with strong repulsions between dissociated carboxylate groups of the citrate and Cys or Hcys molecules. The results of molecular dynamics simulations and quantum mechanical calculations obtained are presented below.

In Fig. 11, the interactions of cysteine and homocysteine with citrate ions in a ligand exchange process are analyzed. It is seen that both Cys and Hcys form intermediate surface complexes on approaching to a citrate-capped gold nanoparticle. Within the framework of electrostatic attractions between COO^- group of the nanoparticle shell and NH_3^+ group of the thioaminoacid, a double hydrogen bond is formed for both the Cit-Cys and Cit-Hcys complexes. Immediately seen is, however, a completely different configuration of the thioaminoacid in the surface complex formed. Whereas a cysteine molecule forms a kind of axial (linear) configuration extending out of the citrate protective SAM, the homocysteine tends to bend out of the axial conformation and toward the citrate side-chain and the electrode surface. The lack of flexibility of the cysteine molecule has already been pointed out when comparing ring-forming abilities of these two molecules [32]. Here, the bending toward the citrates side chain results in the substantial difference in the distance of the thiol group to the gold surface. This distance is 0.75 nm for Cit-Cys surface complex and only 0.38 nm for Cit-Hcys complex. This difference can be translated to classifying the thioaminoacid position as being outside of the shell (in the case of cysteine) or inside the shell (in the case of homocysteine). The large difference in the observed light scattering intensity between Cys and Hcys can be explained by easier and faster penetration of Hcys into the citrate-dominated gold nanoparticle shell followed by citrate ligand replacement. After the ligand exchange has been completed, the zwitterion-type interactions begin to operate leading to the nanoparticle assembly and manifested by the sharp increase in the resonance elastic light scattering, as observed experimentally. On the other hand, in the case of cysteine, the ligand exchange process is strongly hindered by cysteine inability to enter the citrate protective shell due to the axial conformation of the surface complex Cit-Cys.

4. Conclusion

The results demonstrate clearly the differences between cysteine and homocysteine in their ability to ligand exchange with non-ionic

fluorosurfactant-capped AuNP, as well as with negatively charged citrate-capped AuNP. These intriguing differences appear as an amplification of a small structural difference in the molecular build-up (one methylene group), which progresses through several stages leading to the final sensitive detection in the gold nanoparticle assembly process. The selective stages include kinetic retardation due to interactions of the thioaminoacids with the fluorosurfactant chain or formation of charge-induced H-bonded complexes, as in the case of citrate-capped AuNP. Conformational differences in these surface complexes on one hand prevent cysteine from entering the citrate shell and on the other hand pull the homocysteine into the citrate film, thus shortening the distance between the thiol part of the biomarker and the Au surface and making it easier to form Au thiolate bond. We have observed for the first time the RELS characteristics for de-aggregation of citrate-capped gold nanoparticle ensembles followed by their conversion to citrate-linked Hcys-capped nanoparticle assemblies. The ligand exchange effects and gold nanoparticle assembly induced by thioaminoacid zwitterionic interparticle interactions are important in understanding physicochemical aspects of small biomolecule interactions with metal nanoparticles as the use of the latter is widely being explored for new nanomedical applications. The observed differences in the behavior of structurally similar cysteine and homocysteine have profound implications in their analytical determinations using rapid and inexpensive measurement techniques important for the oxidative stress screening and prevention of environmental pollution effects on human health.

Acknowledgements

This work was supported by the U.S. DoD Research Program “Idea”, Grant No. AS-073218.

References

[1] M. Noble, M. Mayer-Proschel, C. Proschel, Redox regulation of precursor cell function: insights and paradoxes, Antioxid. Redox Signal. 7 (2005) 1456–1467.
[2] D. Armstrong, Book oxidative stress biomarkers and antioxidant protocols, Humana Press, Totowa, NJ, 2002.
[3] M.D. Carlo, R.F. Loeser, Increased oxidative stress with aging reduces chondrocyte survival, Arthritis Rheum. 48 (2003) 3419–3430.
[4] S.J. James, S. Melnyk, S. Jernigan, M.A. Cleves, C.H. Halsted, D.J. Wong, P. Cutler, M. Boris, K. Bock, J.J. Bradstreet, S.B. Baker, D.W. Gaylor, Metabolic endophenotype and related genotypes are associated with oxidative stress in children with autism, Am. J. Med. Genet. 141B (2006) 947–956.
[5] Y. Yamamoto, S. Yamanashi, Ubiquinol/ubiquinone ratio as a marker of oxidative stress, in: D. Armstrong (Ed.), Oxidative Stress Biomarkers and Antioxidant Protocols, Humana Press, Totowa, NJ, 2002.
[6] W. Droge, Free radicals inthe physiologic control of cell function, Physiol. Rev. 82 (2002) 47–95.
[7] R. Carmel, D.W. Jacobsen, Book homocysteine in health and disease, Cambridge University Press, Cambridge, U.K., 2001.
[8] D.W. Jacobsen, Hyperhomocysteinemia and oxidative stress: time for a reality check? Arterioscler. Thromb. Vasc. Biol. 20 (2000) 1182–1184.
[9] H. Refsum, P.M. Ueland, O. Nygard, S.E. Volset, Homocysteine and cardiovascular disease, Annu. Rev. Med. 49 (1989) 31.
[10] X. Zhang, H. Li, H. Jin, Z. Ebin, S. Brodsky, M.S. Goligorsky, Effects of homocysteine on endothelialnitric oxide production, Am. J. Physiol. Renal Physiol. 279 (2000) F671.
[11] C. Boushey, S. Beresford, G. Omenn, A. Motulsky, A quantitative assessment of plasma homocysteine as a risk factor for vascular disease: probable benefits of increasing folic acid intake, JAMA 274 (1995) 1049.
[12] I.M. Graham, L. Daly, H. Refsum, K. Robinson, L. Brattstrom and P.M. Ueland, Plasma homocysteine as a risk factor for vascular disease: the European concerted action project, JAMA 277 (1997) 1775; 5482.
[13] S.R. Lentz, W.G. Haynes, Homocysteine: Is it a clinically important cardiovascular risk factor? Clevel. Clin. J. Med. 71 (2004) 729–734.
[14] G.N. Welch, J. Loscalzo, Homocysteine and atherothrombosis, N. Engl. J. Med. 338 (1998) 1042–1050.
[15] S. Seshadri, A. Beiser, J. Selhub, P.F. Jaques, I.H. Rosenberg, R.B. D'Agostino, P.W.F. Wilson, Plasma homocysteine as a risk factor for dementia and Alzheimer's disease, N. Engl. J. Med. 346 (2002) 476.
[16] S. Varadarajan, J. Kanski, M. Aksenova, C. Lauderback, D.A. Butterfield, Different mechanisms of oxidative stress and neurotoxicity for Alzheimer's Ab(1–42) and Ab(25–35), J. Am. Chem. Soc. 123 (2001) 5625.
[17] J.L. Mills, J.M. Scott, P.N. Kirke, J.M. McPartlin, M.R. Conley, D.G. Weir, A.M. Molloy, Y.J. Lee, Homocysteine and neural tube defects, J. Nutr. 126 (1996) S756.
[18] K.M. Beard, N. Shangari, B. Wu, P.J. O'Brien, Metabolism, not autoxidation, plays a role in α-oxoaldehyde- and reducing sugar-induced erythrocyte GSH depletion: Relevance for diabetes mellitus, Mol. Cell. Biochem. 252 (2003) 331–338.
[19] S. Bernard, A. Enayati, L. Redwood, H. Roger, T. Binstock, Autism: a novel form of mercury poisoning, Med. Hypotheses 56 (2001) 462–471.
[20] T. Clark-Taylor, Is autism a disorder of fatty acid metabolism? Possible dysfunction of mitochondrial β-oxidation by long chain acyl-CoA dehydrogenase, Med. Hypotheses 62 (2003) 970–975.
[21] C.V. Guldener, K. Robinson, Homocysteine and renal disease, Semin. Thromb. Hemost. 26 (2000) 313.
[22] B. Brown, Homocysteine: a risk factor for retinal venous occlusive desease, Am. Acad. Ophthalmol. 109 (2002) 287–290.
[23] M. Stobiecka, J. Deeb, M. Hepel, Molecularly-templated polymer matrix films for biorecognition processes: sensors for evaluating oxidative stress and redox buffering capacity, Electrochem. Soc. Trans. 19 (2009).
[24] W. Wang, O. Rusin, X. Xu, K. Kyu, K. Kim, J.O. Escobedo, S.O. Fakayode, K.A. Fletcher, M. Lowry, C.M. Schowalter, C.M. Lawrence, F.R. Fronczek, I.M. Warner, R.M. Strongin, Detection of homocysteine and cysteine, J. Am. Chem. Soc. 127 (2005) 15949–15958.
[25] J.O. Escobedo, O. Rusin, W. Wang, O. Alptürk, K.K. Kim, X. Xu, R.M. Strongin, Detection of biological thiols, Reviews in Fluorescence, Springer, US, 2006, pp. 139–162.
[26] F. Tanaka, N. Mase, C.F. Barbas III, Determination of cysteine concentration by fluorescence increase: reaction of cysteine with a fluorogenic aldehyde, Chem. Commun. 7 (2004) 1762–1763.
[27] E.J. Pacsial-Ong, R.L. McCarley, W. Wang, R.M. Strongin, Electrochemical detection of glutathione using redox indicators, Anal. Chem. 78 (2006) 7577–7581.
[28] L. Agüí, C. Peña-Farfal, P. Yáñez-Sedeño, J.M. Pingarrón, Electrochemical determination of homocysteine at a gold nanoparticle-modified electrode, Talanta 74 (2007) 412–420.
[29] I.I.S. Lim, W. Ip, E. Crew, P.N. Njoki, D. Mott, C.J. Zhong, Y. Pan, S. Zhou, Homocysteine-mediated reactivity and assembly of gold nanoparticles, Langmuir 23 (2007) 826–833.
[30] A.T. Gates, S.O. Fakayode, M. Lowry, G.M. Ganea, A. Marugeshu, J.W. Robinson, R.M. Strongin, I.M. Warner, Gold nanoparticle sensor for homocysteine thiolactone-induced protein modification, Langmuir 24 (2008) 4107–4113.
[31] P.K. Sudeep, S.T.S. Joseph, K.G. Thomas, Selective detection of cysteine and glutathione using gold nanorods, J. Am. Chem. Soc. 127 (2005) 6516–6517.
[32] H.P. Wu, C.C. Huang, T.L. Cheng, W.L. Tseng, Sodium hydroxide as pretreatment and fluorosurfactant-capped gold nanoparticles as sensor for the highly selective detection of cysteine, Talanta 76 (2008) 347–352.
[33] M. Wasowicz, S. Viswanathan, A. Dvornyk, K. Grzelak, B. Kludkiewicz, H. Radecka, Comparison of electrochemical immunosensors based on gold nanomaterials and immunoblot techniques for detection of histidine-tagged proteins in culture medium, Biosens. Bioelectron. 24 (2008) 284–289.
[34] M. Hepel, J. Dallas, M.D. Noble, Interactions and reactivity of Hg(II) on glutathione modified gold electrode studied by EQCN technique, J. Electroanal. Chem. 622 (2008) 173–183.
[35] M. Hepel, E. Tewksbury, Ion-gating phenomena of self-assembling glutathione films on gold piezoelectrodes, J. Electroanal. Chem. 552 (2003) 291–305.
[36] M. Hepel, E. Tewksbury, Nanogravimetric study of templated copper deposition in ion-channels of self-assembled glutathione films on gold piezoelectrodes, Electrochim. Acta 49 (2004) 3827–3840.
[37] S.I. Lim, C.J. Zhong, Molelucarly mediated processing and assembly of nanoparticles: exploring the interparticle interactions and structures, Acc. Chem. Res. 42 (2009) 798–808.
[38] N.N. Kariuki, J. Luo, L. Han, M.M. Maye, L. Moussa, M. Patterson, U. Lin, M.H. Engelhard, C.J. Zhong, Nanoparticle-structured ligand framework as electrode interfaces, Electroanalysis 16 (2004) 120–126.
[39] I.I.S. Lim, C.J. Zhong, Molecularly-Mediated Assembly of Gold Nanoparticles, Gold Bulletin 40/1 (2007) 59–66.
[40] S. Zhang, X. Kou, Z. Yang, Q. Shi, G.D. Stucky, L. Sun, J. Wang, C. Yan, Nanoneckles assembled from gold rods, spheres, and bipyramids, Chem. Commun. (2007) 1816–1818.
[41] L. Han, J. Luo, N. Kariuki, M.M. Maye, V.W. Jones, C.J. Zhong, Novel interparticle spatial properties of hydrogen-bonding mediated nanoparticle assembly, Chem. Mater. 15 (2003) 29–37.
[42] W. Zheng, M.M. Maye, F.L. Leibowitz, C.J. Zhong, Imparting biomimetic ion-gating recognition properties to electrodes with a hydrogen-bonding structured core-shell nanopartricle network, Anal. Chem. 72 (2000) 2190–2199.
[43] I.I.S. Lim, D. Mott, W. Ip, P.N. Njoki, Y. Pan, S. Zhou, C.J. Zhong, Interparticle interactions of glutathione mediated assembly of gold nanoparticles, Langmuir 24 (2008) 8857–8863.
[44] Z.P. Li, X.R. Duan, C.H. Liu, B.A. Du, Selective determination of cysteine by resonance light scattering technique based on self-assembly of gold nanoparticles, Anal. Biochem. 351 (2006) 18–25.
[45] O. Rusin, N.N.S. Luce, R.A. Agbaria, J.O. Escobedo, S. Jiang, I.M. Warner, F.B. Dawan, K. Lian, R.M. Strongin, Visual detection of cysteine and homocysteine, J. Am. Chem. Soc. 126 (2004) 438–439.
[46] F.X. Zhang, L. Han, L.B. Israel, J.G. Daras, M.M. Maye, N.K. Ly, C.J. Zhong, Colorimetric detection of thiol-containing amino acids using gold nanoparticles, Analyst 127 (2002) 462–465.
[47] C. Lu, Y. Zu, V.W.W. Yam, Nonionic surfactant-capped gold nanoparticles as postcolumn reagents for high-performance liquid chromatography assay of low-molecular-mass biothiols, J. Chromatogr. A 1163 (2007) 328–332.

[48] A. Mocanu, I. Cernica, G. Tomoaia, L.D. Bobos, O. Horovitz, M. Tomoaia-Cotisel, Self-assembly characteristics of gold nanoparticles in the presence of cysteine, Colloids Surf. A 338 (2009) 93–101.
[49] W. Wang, J.O. Escobedo, C.M. Lawrence, R.M. Strongin, Direct detection of homocysteine, J. Am. Chem. Soc. 126 (2004) 3400–3401.
[50] M.J. Hostetler, A.C. Templeton, R.W. Murray, Dynamics of place-exchange reactions on monolayer-protected gold cluster molecules, Langmuir 15 (1999) 3782–3789.
[51] M.J. Hostetler, J.E. Wingate, C.J. Zhong, J.E. Harris, R.W. Vachet, M.R. Clark, J.D. Londono, S.J. Green, J.J. Stokes, G.D. Wignall, J.L. Glish, M.D. Porter, N.D. Evans, R.W. Murray, Alkanethiolate gold cluster molecules with core diameters from 1.5 to 5.2 nm: core and monolayer properties as a function of core size, Langmuir 14 (1998) 17–30.
[52] C. Lu, Y. Zu, V.W.W. Yam, Specific postcolumn detection method for HPLC assay of homocysteine based on aggregation of fluorosurfactant-capped gold nanoparticles, Anal. Chem. 79 (2007) 666–672.
[53] C.C. Huang, W.L. Tseng, Role of fluorosurfactant-modified gold nanoparticles in selective detection of homocysteine thiolactone: remover and sensor, Anal. Chem. 80 (2008) 6345–6350.
[54] C.J. Ackerson, M.T. Sykes, R.D. Kornberg, Liagnd exchange between GSH and thiolated oligonucleotides on AuNP, Proc. Natl. Acad. Sci. U.S.A. 102 (2005) 13383.
[55] B.T. Draine, P.J. Flatau, Discrete-dipole approximation for scattering calculations, J. Opt. Soc. Am. A 11 (1994) 1491–1499.
[56] W.H. Yang, G.C. Schatz, R.R.v. Duyne, Discrete dipole approximation for calculating extinction and Raman intensities for small particles with arbitrary shapes, J. Chem. Phys. 103 (1995) 869–875.
[57] A. Brioude, X.C. Jiang, M.P. Pileni, Optical properties of gold nanorods: DDA simulations supported by experiments, J. Phys. Chem. B 109 (2005) 13138–13142.
[58] K.S. Lee, M.A. El-Sayed, Dependence of the enhanced optical scattering efficiency relative to that of absorption for gold metal nanorods on aspect ratio, size, end-cap shape, and medium refractive index, J. Phys. Chem. B 109 (2005) 20331.
[59] P.K. Jain, K.S. Lee, I.H. El-Sayed, M.A. El-Sayed, Calculated absorption and scattering properties of gold nanoparticles of different size, shape, and composition: applications in biological imaging and biomedicine, J. Phys. Chem. B 110 (2006) 7238.
[60] E.S. Kooij, B. Poelsema, Shape and size effects in the optical properties of metallic nanorods, Phys. Chem. Chem. Phys. 8 (2006) 3349–3357.
[61] K.S. Lee, M.A. El-Sayed, Gold and silver nanoparticles in sensing and imaging: sensitivity of plasmon response to size, shape, and metal composition, J. Phys. Chem. B 110 (2006) 19220.
[62] S.W. Prescott, P. Mulvaney, Gold nanorod extinction spectra, J. Appl. Phys. 99 (2006) 123504.
[63] G. Yin, S.Y. Wang, M. Xu, L.Y. Chen, discrete dipole approximation — size and shape, J. Korean Phys. Soc. 49 (2006) 2108.
[64] A.L. Gonzales, C. Noguez, Influence of morphology on the optical properties of metal nanoparticles, J. Comput. Theor. Nanosci. 4 (2007) 231.
[65] C. Ungureanu, R.G. Rayavarapu, S. Manohar, T.G.v. Leeuwen, Discrete dipole approximation simulations of gold nanorod optical properties: choice of input parameters and comparison with experiment, J. Appl. Phys. 105 (2009) 102032.
[66] P.B. Johnson, R.W. Christy, Optical constants of the noble metals, Phys. Rev. B 6 (1972) 4370.
[67] M.M. Alvarez, J.T. Khoury, T.G. Schaaff, M.N. Shafigullin, I. Vezmar, R.L. Whetten, Optical absorption spectra of nanocrystal gold molecules, J. Phys. Chem. B 101 (1997) 3706–3712.
[68] S. Link, M.A. El-Sayed, Spectral properties and relaxation dynamics of surface plasmon electronic oscillations in gold and silver nanodots and nanorods, J. Phys. Chem. B 103 (1999) 8410–8426.
[69] S. Link, M.B. Mohamed, M.A. El-Sayed, Simulation of the optical absorption spectra of gold nanorods as a function of their aspect ratio and the medium dielectric constant, J. Phys. Chem. B 103 (1999) 3073–3077.
[70] P.V. Kamat, Photophysical, photochemical and photocatalytic aspects of metal nanoparticles, J. Phys. Chem. B 106 (2002) 7729–7744.
[71] M. Mishchenko, L. Travis, A. Lacis, Scattering, absorption, and emission of light by small particles, Cambridge University Press, Cambridge, 2002.
[72] J. Perez-Juste, I. Pastoriza-Santos, L.M. Liz-Marzan, P. Mulvaney, Gold nanorods: Synthesis, characterization and applications, Coord. Chem. Rev. 249 (2005) 1870–1901.
[73] P.G. Etchegoin, E.C.l. Ru, M. Meyer, An analytic model for the optical properties of gold, J. Chem. Phys. 125 (2006) 164705-1–164705-3.
[74] Y. Ping, D. Hanson, I. Koslov, T. Ogitsu, O. Prendergast, E. Schwegler, G. Collins, A. Ng, Dielectric function of warm dense gold, Phys. Plasmas 15 (2008) 056303.
[75] R.F. Pasternack, C. Bustamante, P.J. Collings, A. Giannetto, E.J. Gibbs, Porphyrin assemblies on DNA as studied by a resonance light-scattering technique, J. Am. Chem. Soc. 115 (1993) 5393–5399.
[76] R.F. Pasternack, Resonance light scattering: a new technique for studying chromophore aggregation, Science 269 (1995) 935.
[77] C.Z. Huang, K.A. Li, S.Y. Tong, Determination of nanogram of nucleic acids by their enhancement effect on the resonance light scattering of the cobalt(II)/4-[(5-chloro-2-pyridyl)azo]-1, 3-diaminobenzene complex, Anal. Chem. 69 (1997) 514–520.
[78] C.Z. Huang, K.A. Li, S.Y. Tong, Determination of nucleic acids by a resonance light-scattering technique with a, b, c, d-tetrakis[4-(trimethylammoniumyl)phenyl] porphine, Anal. Chem. 68 (1996) 2259–2263.
[79] Z.X. Guo, H.X. Shen, Sensitive and simple determination of protein by resonance Rayleigh scattering with 4-azochromotropic acid phenylfluorone, Anal. Chim. Acta 408 (2000) 177–182.
[80] Y.T. Wang, F.L. Zhao, K.A. Li, S.Y. Tong, Molecular spectroscopic study of DNA binding with neutral red and application to assay of nucleic acids, Anal. Chim. Acta 396 (1999) 75–81.
[81] C.Z. Huang, Y.F. Li, X.D. Liu, Determination of nucleic acids at nanogram levels with safranine T by a resonance light-scattering technique, Anal. Chim. Acta 375 (1998) 89–97.
[82] Y. Liu, C.Q. Ma, K.A. Li, F.C. Xie, S.Y. Tong, Rayleigh light scattering study on the reaction of nucleic acids and methyl violet, Anal. Biochem. 268 (1999) 187–192.
[83] X. Wu, Y. Wang, M. Wang, S. Sun, J. Yang, Y. Luan, Determination of nucleic acids at nanogram level using resonance light scattering technique with Congo Red, Spectrochim. Acta A 61 (2005) 361–366.
[84] Z. Jia, J. Yang, X. Wu, C. Sun, S. Liu, F. Wang, Z. Zhao, The sensitive determination of nucleic acids using resonance light scattering quenching method, Spectrochim. Acta A 64 (2006) 555–559.
[85] D.E. Aspnes, Effective medium theory, Am. J. Phys. 50 (1982) 704.
[86] K.L. Kelly, E. Coronado, L.L. Zhao, G.C. Schatz, The optical properties of metal nanoparticles: the influence of size, shape, and dielectric environment, J. Phys. Chem. B 107 (2003) 668–677.
[87] J. Nappa, G. Revillod, J.P. Abid, I. Russier-Antoine, C. Jonin, E. Benichou, H.H. Girault, P.F. Brevet, Hyper-Rayleigh scattering of gold nanorods and their relationship with linear assemblies of gold nanospheres, Faraday Discuss. 125 (2004) 145–156.
[88] J. Turkevich, P.C. Stevenson, J. Hiller, synthesis of AuNP, Discuss. Faraday Soc. 11 (1951) 55–75.
[89] W.J. Hehre, L. Radon, P.R. Schleyer, J.A. Pople, Ab-initio molecular orbital theory, Wiley, New York, 1985.
[90] P.W. Atkins, R.S. Friedman, Molecular quantum mechanics, Oxford University Press, Oxford, 2004.
[91] F. Li, Y. Zu, Effect of nonionic fluorosurfactant on the electrogenerated chemiluminescence of the Tris (2, 2′-bipyridine)ruthenium(II)/Tri-n-propylamine system: lower oxidation potential and higher emission intensity, Anal. Chem. 76 (2004) 1768–1772.
[92] R. Elghanian, J.J. Storhoff, R.C. Mucic, R.L. Letsinger, C.A. Mirkin, Selective colorimetric detection of polynucleotides based on the distance-dependent optical properties of gold nanoparticles, Science 277 (1997) 1078–1081.
[93] A.P. Alivisatos, K.P. Johnsson, X. Peng, T.E. Wilson, C.J. Loweth, M.P. Bruchez, P.G. Schultz, attachment of oligonucleotides to thiol-coated AuNP, Nature 382 (1996) 610.
[94] M.M. Maye, I.I.S. Lim, J. Luo, Z. Rab, D. Rabinovich, T. Liu, C.J. Zhong, Mediator-template assembly of nanoparticles, J. Am. Chem. Soc. 127 (2005) 1519–1529.
[95] S.J. Park, T.A. Taton, C.A. Mirkin, Array-based electrical detection of DNA with nanoparticle probes, Science 295 (2002) 1503–1505.
[96] R.A. Reynolds, C.A. Mirkin, R.L. Letsinger, Homogeneous, nanoparticle-based quantitative colorimetric detection of oligonucleotides, J. Am. Chem. Soc. 122 (2000) 3795–3796.
[97] J.J. Storhoff, R. Elghanian, R.C. Mucic, C.A. Mirkin, R.L. Letsinger, One-pot colorimetric differentiation of polynucleotides with single base imperfections using gold nanoparticle probes, J. Am. Chem. Soc. 120 (1998) 1959–1964.
[98] T.A. Taton, G. Lu, C.A. Mirkin, Two-color labeling of oligonucleotide arrays via size-selective scattering of nanoparticle probes, J. Am. Chem. Soc. 123 (2001) 5164–5165.
[99] T.A. Taton, R.C. Mucic, C.A. Mirkin, R.L. Letsinger, The DNA-mediated formation of supramolecular mono- and multilayered nanoparticle structures, J. Am. Chem. Soc. 122 (2000) 6305–6306.